

GREEN SYNTHESIS OF MANGANESE OXIDE NANOPARTICLES USING ANTHOCYANIN EXTRACT FOR THE SEQUESTRATION OF CRYSTAL VIOLET DYE

**Thesis Submitted
in Partial Fulfillment of the Requirements for the
Degree of**

**MASTER OF SCIENCE
in
CHEMISTRY**

Submitted by

**AAKASH
2K23/MSCCHE/65**

**Under the supervision of
DR. RAMINDER KAUR**



**DEPARTMENT OF APPLIED CHEMISTRY
DELHI TECHNOLOGICAL UNIVERSITY
BAWANA ROAD, Delhi-110042
JUNE, 2025**

DELHI TECHNOLOGICAL UNIVERSITY
(Formerly Delhi College of Engineering)
Shahbad Daultpur, Main Bawana Road, Delhi-42

ACKNOWLEDGEMENTS

The success of this project was made possible with the invaluable guidance and assistance from many individuals and support from numerous individuals, and we are quite grateful to have had this throughout the dissertation process.

I express my sincere gratitude to my project supervisor, **Dr. Raminder Kaur**, Department of Applied Chemistry, Delhi Technological University, for her valuable guidance and unwavering support throughout the course of this project. I thank **Prof. Anil Kumar**, Head of the Department of Applied Chemistry, for his unwavering inspiration. My deepest gratitude goes to **Prof. Ram Singh** for his invaluable help and advice. I am also grateful to all the teaching staff of the Department for their guidance, support, and encouragement throughout this project. And sincere thanks to the Ph.D. Research Scholar's, **Ms. Sarla Yadav, Ms. Gunjan Varshney, Ms. Pooja Yadav, and Ms. Shikha Jain** for their continuous support and assistance.

Lastly, I would like to express my sincere gratitude to my family and friends for their continuous encouragement and support, which enabled us to persevere through the hard workdays.

AAKASH

DELHI TECHNOLOGICAL UNIVERSITY
(Formerly Delhi College of Engineering)
Bawana Road, Delhi-110042

CANDIDATE'S DECLARATION

I, AAKASH (2k23/MSCCHE/65) students of M.Sc. (Applied Chemistry), hereby declare that the project Dissertation titled **“GREEN SYNTHESIS OF MANGANESE OXIDE NANOPARTICLES USING ANTHOCYANIN EXTRACT FOR THE SEQUESTRATION OF CRYSTAL VIOLET DYE”**, which is submitted by me to the Department of Applied Chemistry, Delhi Technological University, Delhi in partial fulfilment of the requirement for the award of the degree of Master of Science, is original and not copied from any source without proper citation. This work has not previously formed the basis for the award of any Degree, Diploma, Associateship, Fellowship or other similar title or recognition.

Place : Delhi

AAKASH

Date : 20-06-2025

DELHI TECHNOLOGICAL UNIVERSITY
(Formerly Delhi College of Engineering)
Bawana Road, Delhi-110042

CERTIFICATE

I hereby certify that the Project Dissertation titled “**GREEN SYNTHESIS OF MANGANESE OXIDE NANOPARTICLES USING ANTHOCYANIN EXTRACT FOR THE SEQUESTRATION OF CRYSTAL VIOLET DYE**” which is submitted by Mr. Aakash (2k23/MSCCHE/65) student of M.Sc. (Applied Chemistry) Delhi Technological University, Delhi in partial fulfilment of the requirement for the award of the degree of Master of Science, is a record of the project work carried out by the students under my supervision. To the best of my knowledge this work has not been submitted in part or full for any Degree or Diploma to this University or elsewhere.

Place: Delhi
Date: 20-06-2025

DR. RAMINDER KAUR
SUPERVISOR

Abstract

Crystal Violet (CV) is a synthetic triphenylmethane dye that is widely used in biomedical staining, printing, and textile processing. Because of its great chemical stability, CV is a persistent pollutant in industrial effluent streams and is known to have hazardous and carcinogenic effects despite its usefulness. To address this concern, this study focuses on the Green Synthesis of Manganese oxide (MnATH-(O) NPs) utilizing anthocyanin (ATH) extract obtained from red cabbage, which serves as a stabilizing, capping, and reducing agent. The physiochemical properties of the green synthesized MnATH-(O) NPs were extensively analysed using multiple characterization techniques. Powder X-ray diffraction was employed to confirm the crystalline phase and estimate the average crystallite size, while Fourier Transform Infrared Spectroscopy (FTIR) was used to identify the surface functional groups involved in nanoparticle stabilization. The characterization results revealed that the synthesized material possessed a crystallite size of 20.3 nm, indicative of high crystallinity and phase purity. Additionally, the measured surface charge of -34.7 mV suggests strong electrostatic affinity toward positively charged azo dye molecules, supporting its potential as an efficient adsorbent in wastewater treatment applications. Batch adsorption experiments were conducted under varying conditions of initial dye concentration, contact time, adsorbent dosage and pH to optimize dye removal efficiency, attaining a removal efficiency of 98.36% within 60 minutes. The adsorption kinetics were best described by pseudo-second-order model demonstrating that the chemisorption was the predominant mechanism governing the interaction between MnO nanoparticles. Additionally, the equilibrium data fitted well with the Temkin isotherm model, suggesting multilayer adsorption on a heterogeneous surface. These findings highlight the potential of green-synthesised MnO nanoparticles as an environmentally friendly and highly effective adsorbent for the removal of cationic dyes. In addition to reducing environmental effect, using an eco-friendly synthesis process improves surface characteristics that are conducive to adsorption. Overall, this study shows a viable, affordable wastewater treatment method that might be scaled up and used in actual effluent systems.

TABLE OF CONTENTS

S.No.	Topic		Page No.
a.	<i>Acknowledgments</i>		<i>ii</i>
b.	<i>Declaration</i>		<i>iii</i>
c.	<i>Certificate</i>		<i>iv</i>
d.	<i>Abstract</i>		<i>v</i>
e.	<i>Contents</i>		<i>vi</i>
f.	<i>List of Tables</i>		<i>viii</i>
g.	<i>List of Figures</i>		<i>ix</i>
h.	<i>List of abbreviations and symbols, and nomenclature</i>		<i>x</i>
1	CHAPTER 1: INTRODUCTION AND LITERATURE SURVEY		1-4
2	CHAPTER 2: EXPERIMENTAL SECTION		5-9
	2.1	CHEMICALS REQUIRED	5
	2.2	METHODOLOGY	5
	2.2.1	Preparation of Anthocyanin Extract (ATH)	5
	2.2.2	Synthesis of Manganese MnO	5
	2.2.3	Synthesis of Manganese MnATH-(O) NPs	6
	2.3	ADSORPTION STUDY	6
	2.4	CHARACTERIZATION TECHNIQUES	7
	2.4.1	PXRD Analysis	7
	2.4.2	Fourier Transform Infrared Spectroscopy (FTIR)	9
3	CHAPTER 3: RESULTS AND DISCUSSIONS		10-23
	3.1	CHARACTERIZATION	10
	3.1.1	XRD Analysis	10
	3.1.2	FTIR Analysis	11
	3.2	BATCH ADSORPTION EXPERIMENTS	12
	3.2.1	Impact of Contact time on CV dye	13

	3.2.2	Impact of Initial CV dye concentration	14
	3.2.3	Impact of adsorbent dosage	14
	3.2.4	Impact of pH on CV dye solution	14
3.3	ADSORPTION KINETICS		15
	3.3.1	Pseudo-first-order (PFO) Adsorption Kinetics Model	15
	3.3.2	Pseudo-second-order (PSO) Adsorption Kinetics Model	15
	3.3.3	Intraparticle Diffusion (IPD) Adsorption Kinetics Model	16
3.4	ADSORPTION ISOTHERM		18
	3.4.1	Langmuir Adsorption Isotherm Model	18
	3.4.2	Freundlich Adsorption Isotherm Model	19
	3.4.3	Temkin Adsorption Isotherm Model	19
3.5	ADSORPTION THERMODYNAMICS		21
4	<i>CHAPTER 4 CONCLUSION AND FUTURE PROSPECTS</i>		24-25
	4.1	CONCLUSION	24
	4.2	FUTURE PROSPECTS	25
5	<i>REFERENCES</i>		26-27
6	<i>PLAGIARISM REPORT</i>		28-32

LIST OF TABLES

- Table 1.1:** Reported Applications of Bio-synthesised MONPs.
- Table 3.3.1:** List of calculated parametric values for adsorption kinetics model for CV dye adsorption by MnATH-(O) NPs
- Table 3.4.1:** Compilation of adsorption isotherm parametric values for several mathematical models
- Table 3.5.1:** Thermodynamic parametric values for CV dye adsorption by MnATH-(O) NPs

LIST OF FIGURES

Figure 2.2.1: Synthesis of MnO NPs with ATH Extract

Figure 2.2.2: Synthesis of MnO NPs

Figure 2.4.1: Digital X-Ray Diffractometer

Figure 2.4.2: Digital FTIR Spectrophotometer

Figure 3.1.1: PXRD pattern of synthesized MnO NPs and MnATH-(O) NPs

Figure 3.1.2: FTIR spectrum of synthesized MnO NPs and MnATH-(O) NPs

Figure 3.2.1: (a) UV Visible spectra of adsorption of CV dye using MnATH-(O) NPs, (b) influence of contact time on removal efficiency, (c) influence of initial dye concentration on adsorption capacity, (d) effect of adsorbent dosage on removal efficiency, Influence of pH on CV dye solution for removal efficiency

Figure 3.3.1: The linear adsorption kinetics curves that were fitted for CV dye adsorption by MnATH-(O) NPs using PFO, PSO and IPD MODEL

Figure 3.4.1: The graphs showing the linear connections between the Temkin, Freundlich, and Langmuir isotherm model

Figure 3.5.1: The Van't Hoff equation plot ($\ln K$ vs $1/T$) and the effect of temperature on adsorption capacity have been presented.

LIST OF ABBREVIATIONS AND SYMBOLS AND NOMENCLATURE

FTIR	Fourier Transform Infrared Spectroscopy
PXRD	Powder X-Ray Diffraction
FE-SE	M Field Emission-Scanning Electron Microscopy
EDX	Energy Dispersive X-Ray
BET	Brunauer-Emmett-Teller
OER	Oxygen evolution reaction
BG	Brilliant green
CR	Congo Red
CV	Crystal Violet
MB	Methylene Blue
MO	Methyl Orange
NaOH	Sodium Hydroxide
MOOH	Metal oxyhydroxide
MnO	Manganese oxide
DI water	Deionized water
g	Grams
K	Kelvin
kJ	kilojoule
min.	Minutes
mV	millivolt
M	Molar
nm	Nanometre
pH	Potential of Hydrogen
rpm	Revolution Per minute
°C	Degree Celsius

CHAPTER 1

INTRODUCTION AND LITERATURE REVIEW

Over the past decades, The rapid growth of cities and factories have resulted in a notable rise in environmental pollution, especially due to the release of toxic pollutants such as dyes, heavy metals, volatile organic compounds, etc., into water bodies. Among various pollutants, synthetic dyes emerged as the most persistent and hazardous contaminant released from textile, leather, paper, printing and cosmetic industries, thus causing adverse impact on the ecosystem [1]. Among the synthetic dyes, crystal violet (CV) dye, a photo-stable azo dye, consists of hexamethyl pararosaniline chloride molecules. CV dye is extremely harmful to animals, exhibiting mutagenic and carcinogenic properties due to its aromatic structure[2], [3], which is resistant to environmental degradation, resulting in respiratory issues, skin and digestive tract irritation, liver, kidney damage and renal failure [4], [5]. The cationic CV dye in water impedes sunlight penetration, hindering the photosynthesis of aquatic plants and hence promoting bacterial proliferation. Consequently, the removal of these cationic azo dyes is critically important for safeguarding ecological balance. As of today, numerous methods for the elimination of these contaminants are reported in the literature, including precipitation, chemical oxidation, photodegradation, coagulation-flocculation, ultra and nanofiltration, membrane filtration, electrolysis, and biological processes. Nonetheless, their practical application remains constrained by specific limitations inherent to traditional methods for azo dye removal, including (i) considerable operational costs due to elevated energy demands, (ii) prolonged duration, (iii) necessity for substantial chemical quantities, (iv) production of detrimental secondary pollutants such as sludge and novel hazardous compounds, (v) insufficient dye removal leading to contaminated influents, and (vi) prohibited effectiveness.

In recent years, adsorption has come into focus as a promising technique for wastewater treatment, owing to its simplicity, versatility, effectiveness, and cost-efficiency. The adsorptive removal of pollutants depends on the solid-liquid intermolecular attraction between the adsorbate and the adsorbent, facilitating the transfer of pollutants from the aqueous solution to the adsorbent's surface. Currently, a diverse array of substances serves as adsorbents, including carbon-based compounds, biosorbents, silicon-based materials, zeolites, organic polymers, natural clays, metal

hydroxides, and agricultural wastes, for the removal of dyes, metals, pesticides, and phenolic compounds from water sources [6]. The practical application of these materials remains limited due to high costs, insufficient adsorption capacities, and difficulties in their reuse and regeneration. Recently, transition metal oxides (TMOs) have attracted significant attention owing to their compositional diversity, high surface area to volume ratio, non-toxic, enhanced reactivity, and prospective applications across various fields (sensing, wastewater treatment, energy storage, etc) (Table 1.1). The synthesis of MONPs can be achieved through various top-down and bottom-up methodologies, including sol-gel, hydrothermal, microwave irradiation, laser ablation, and chemical reduction techniques. Conventional methods exhibit limitations related to the use of hazardous precursors, high costs, time consumption, energy intensity, and the generation of toxic byproducts, which pose significant challenges to sustainability and environmental safety. To address this issue, researchers have chosen a more environmentally friendly approach that eliminates the need for toxic chemicals and energy-intensive methods. Researchers have explored various bioresources for green synthesis, including plant components such as leaves, bark, roots, stems, seeds, flowers, fruits, and tubers, microorganisms like algae, fungi, and bacteria. Plant-derived bioresources are preferred due to their rich content of bioactive compounds, including alkaloids, flavonoids, terpenoids, and triterpenoids, which function as natural capping and reducing agents in nanoparticle synthesis. Plant extracts containing bioactive compounds, particularly anthocyanins (ATH), have shown significant potential in the biosynthesis of nanoparticles (NPs) among various natural sources [6].

ATH is prevalent in RC and serves dual roles as both reducing and capping agents. Consequently, its antioxidant qualities enhance the stability and performance of nanoparticles [7]. The process involves phytochemicals in the extract mediating the reduction of manganese ions to manganese oxide, which produces nanoparticles with controlled size and shape. Red cabbage's high ATH content, affordability, and availability make it a good choice for this use [8]. RC is the source of ATH extract, which has a high concentration of several phytochemicals and minerals, including Vitamin C and K, β -carotene, minerals, fibers, total polyphenols, and glucosinolates. ATHs represent the glycosylated derivatives of anthocyanidins (aglycones) [9]. The ATH extract contains key functional groups, specifically hydroxyl (-OH) and methoxy (-OCH₃) groups, which are attached to phenolic rings and play a significant role in its antioxidant properties. ATH includes glycosidic bonds that link sugars such as glucose or galactose to aglycones, thereby improving

their solubility and stability in aqueous environments. The inclusion of carbonyl (C=O) groups in the core structure enhances the electron configuration [10]. ATH derived from RC exhibits strong reducing properties and the ability to chelate metal ions, making it highly effective in the synthesis of nanoparticles. The use of RC extract is consistent with green chemistry principles, as it removes the need for hazardous chemicals and reduces the overall environmental impact of the synthesis process. ATH extracted from RC demonstrates significant versatility and effectiveness, offering potential for the synthesis of MnO nanoparticles with enhanced photocatalytic properties.

This study presents Anthocyanin mediated synthesis of manganese oxides (MnATH-(O) NPs) for applications in wastewater treatment. The physiochemical properties of the synthesized material were analysed using Powder X-ray Diffraction (PXRD), Fourier Transform Infrared Spectroscopy (FTIR), Field Emission-Scanning Electron Microscopy with Energy Dispersive X-ray Spectroscopy (FESEM with EDX), analysis, and Dynamic Light Scattering (DLS). The results indicate that the synthesized material has a crystallite size of 20.3 nm, suggesting high purity and crystallinity. The synthesized material exhibits a negative surface charge of -34.7 mV, indicating effectiveness in the adsorption of cationic azo dyes. The synthesized materials were subsequently employed as adsorbents for the effective removal of CV dye from wastewater, attaining a removal efficiency of 98.36% within 60 minutes. Adsorption studies were conducted by varying parameters such as contact time, initial dye concentration, adsorbent dosage, pH, and temperature. The adsorption mechanism was elucidated using the pseudo-second order kinetic model, indicating the chemical adsorption of CV dye onto the MnATH-(O) NPs surface. The non-homogeneous and multilayer adsorption type is, to our knowledge, the most efficient, demonstrating a maximum uptake capacity of 49.039 mg g⁻¹ for CV dye on MnATH-(O) NPs. This synthesis method is regarded as environmentally sustainable within the framework of environmental remediation, particularly concerning waste management protocols.

Table 1.1: Reported Applications of Bio-synthesized MONPs

MONPs	Biological methods	Parts	Application	References
ZnO NPs	Fungus	Culture filtrate of the endophytic fungus <i>Alternaria tenuissima</i>	Antimicrobial, Antioxidant, Anticancer and Photocatalytic activity	[11]
ZnO and CuO NPs	Plant	Leaf extract of <i>Aloe barbadensis</i>	Water Treatment	[12]
Ag NPs	Animal	Extract from animal fur (Goat)	Water treatment	[13]
ZnO, CuO and Fe ₂ O ₃ NPs	Plant	Leaves of <i>Cassia fistula</i>	Water treatment	[14]
ZnO- CuO NCs	Plant	Leaves of kei apple <i>Dovyalis caffra</i>	Water treatment	[15]
NiO NPs and CuNiO NCs	Plant	Leaf extract of <i>P. dodecandra</i> L'Herit	Water treatment	[16]
Cu and CuO NPs	E-waste	Waste printed circuit boards (WPCBs)	Antibacterial and Photocatalytic activity	[17]

CHAPTER 2

EXPERIMENTAL SECTION

2. REAGENTS AND METHOD

2.1 Chemicals required

The chemical reagents required in this synthesis, Manganese(II) acetate tetrahydrate ($\text{Mn}(\text{CH}_3\text{COO})_2 \cdot 4\text{H}_2\text{O}$) and Sodium hydroxide (NaOH), ($\geq 99\%$ purity), were obtained from MERCK. To extract ATH, red cabbage was purchased from a Delhi, India, local market. Anhydrous ethanol (EtOH) and hydrochloric acid (HCl), were obtained from Thermo Fisher Scientific. Crystal violet (CV) (Hexamethyl pararosaniline chloride ($\text{C}_{25}\text{H}_{30}\text{ClN}_3$)) was purchased from CDH chemicals. and all the experiments were conducted using deionized water (DI).

2.2 METHODOLOGY

2.2.1. Preparation of Anthocyanin Extract (ATH)

ATH was extracted from RC (*Brassica oleracea* var. capitata) via a process analogous to that documented in the literature, employing pure ethanol as the solvent [18].

2.2.2 Chemical Synthesis of Manganese Oxide Nanoparticles (MnO NPs)

A cost-efficient co-precipitation technique was utilized to produce MnO nanoparticles from the precursor ($\text{Mn}(\text{CH}_3\text{COO})_2 \cdot 4\text{H}_2\text{O}$) and NaOH , as illustrated in Figure 2.2.2. 1 g of ($\text{Mn}(\text{CH}_3\text{COO})_2 \cdot 4\text{H}_2\text{O}$) was introduced during the synthesis procedure. A beaker with 50 mL of distilled water was constantly swirled for 15 minutes at room temperature. By gradually adding 1.5 M NaOH solution, the mixture's pH was kept at 9. The resulting mixture was then stirred at 450 rpm for four hours at room temperature. After that, the dark precipitate was filtered and cleaned using distilled water and a 1:1 ethanol solvent. After that, the product was dried in an oven for 24 hours at 60°C . Using a mortar and pestle, the dry product was further grounded into a fine powder before being calcined in a muffle furnace for two hours at 450°C .

2.2.3 Synthesis of Manganese oxide MnATH-(O) NPs

The green synthesis of MnATH-(O) NPs was conducted utilising ATH extract, as illustrated in Figure 2.2.1. Initially, 1 g of $\text{Mn}(\text{CH}_3\text{COO})_2 \cdot 4\text{H}_2\text{O}$ was agitated for 15 minutes at room temperature after dissolving in 50 millilitres of distilled water. Five millilitres of ATH solution were then added, and the mixture was agitated for half an hour. At this point, the colour of the solution turned brown. To keep the pH of the solution at 9, 1.5 M NaOH solution was added dropwise. The mixture was then shaken for four hours. A 1:1 mixture of distilled water and ethanol was then used to filter and rinse the brown precipitate. After being dried for 24 hours at 60 °C, the final product was calcined for two hours at 450 °C in a muffle furnace.

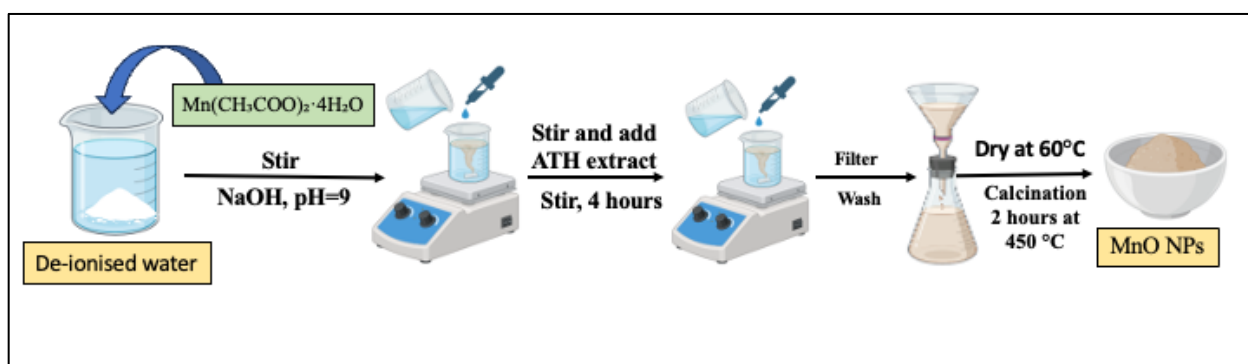


Figure 2.2.1 Synthesis of MnO NPs with ATH Extract

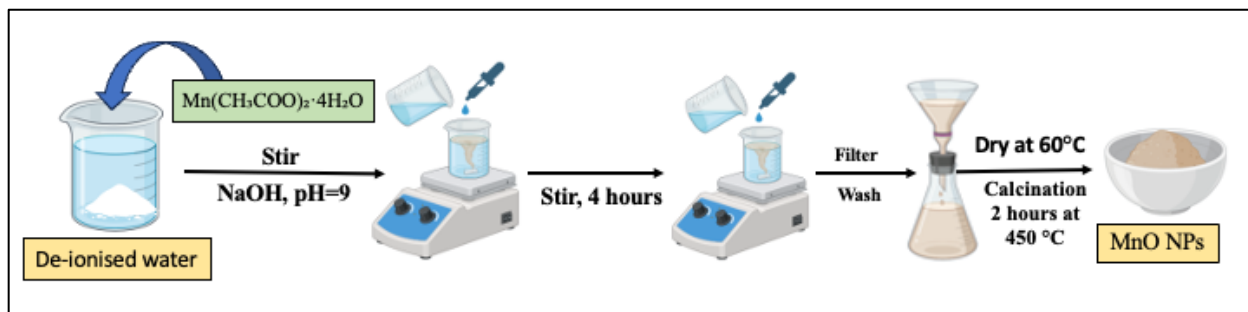


Figure 2.2.2: Synthesis of MnO NPs

2.3 ADSORPTION STUDIES

Adsorption studies were conducted under dark conditions. A number of batch adsorption experiments were performed with varying parameters such as temperature (313.15k - 333.15k), pH (3- 11), initial concentration of CV dye (10 mg L^{-1} - 50 mg L^{-1}), contact time (0 - 60 minutes),

different adsorbent dosage (50 mg – 200 mg). Constant volume of solution was taken at regular intervals of time. Then the samples were centrifuged at 4000 rpm, for 10 minutes. Then the absorbance spectrum was recorded using a Shimadzu1900i UV-vis spectrophotometer at $\lambda_{\text{max}}=579$. The equilibrium dye uptake capacity, q_e (mg g⁻¹), was calculated using:

$$q_e = \frac{C_i - C_e}{W} * V \quad (1)$$

Here, CV dye's initial and equilibrium concentrations are indicated as C_i and C_e (mg L⁻¹). The adsorbent mass is stated as W (mg), whereas V denotes the dye solution's volume (mL). The following expression was used to determine the removal effectiveness for CV dye:

$$\% \text{removal} = \frac{C_i - C_t}{C_i} * 100 \quad (2)$$

The rate-determining step and completion time for the adsorption process were also determined using kinetic models. The following equation was used to calculate the dye absorption capacity at time t .

$$q_t = \frac{C_i - C_t}{W} * V \quad (3)$$

Where, W and V stand for the mass of adsorbent (mg) and the volume of the solution (mL), respectively, and q_t for the quantity of dye adsorbed at time t (mg g⁻¹), C_i and C_t for the initial and final dye concentrations (mg L⁻¹).

2.4.CHARACTERIZATION TECHNIQUES

2.4.1. PXRD Analysis

Using PXRD, the synthesized nanomaterials structural identification and compositional characterization were evolved. The PXRD patterns of MnATH-(O) NPs are displayed in the Figure 3. One method for figuring out the crystal structure of powdered materials is PXRD. A standard digital X-ray diffractometer is depicted in Figure 2.4.1. X-rays are typically produced using revolving anodes, sealed tubes, and synchrotron radiation sources. XRD analysis can be used to study materials like metals, ceramics, polymers, and semiconductors. The method can be applied to characterize new materials, identify unfamiliar materials, and track the quality of materials while they are being manufactured. Crystals scatter X-rays in a characteristic way, which allows for a

structural investigation in XRD analysis. A number of the samples macro and microstructural characteristics can be gleaned from, including:

- **Peak Position:** Phase structure, chemical composition, macro stresses, and lattice parameters are all analyzed using curves.
- **Peak Shape:** Contributes to sample broadening (micro strains and crystallite size)

$$D = 0.94 \lambda / \beta \cos \theta \quad (2)$$

Here, the average crystallinity is D ,
the wavelength is in \AA ,
FWHM is β (in radian) and
 θ indicates the degree of diffraction.



Figure 2.4.1 Digital X-Ray Diffractometer

2.4.2. Fourier Transform Infrared Spectroscopy (FTIR)

An analytical method called FTIR analysis makes use of infrared light to determine and measure the chemical makeup of a material. A digital FTIR spectrophotometer is depicted in Figure 2.4.2. The interaction between a sample and an infrared light beam is measured by FTIR analysis. The spectrum reveals the functional groups present in the samples as well as details about their chemical makeup. Because of this, no two substances have identical infrared spectra. In this sense, an infrared spectrum might serve as a fingerprint for identification. IR spectroscopy can be used to qualitatively analyze a variety of materials. IR is typically divided into three regions: near-IR ($400\text{--}10\text{ cm}^{-1}$), mid-IR ($4000\text{--}400\text{ cm}^{-1}$), and far-IR ($14000\text{--}4000\text{ cm}^{-1}$).

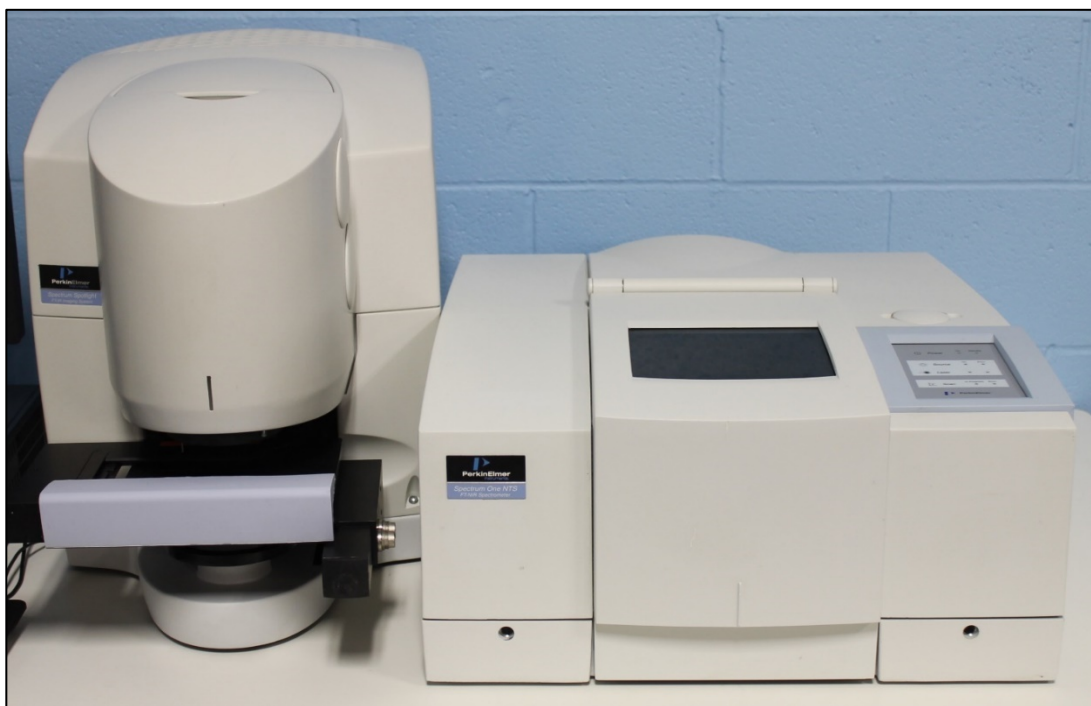


Figure 2.4.2 Digital FTIR Spectrophotometer

CHAPTER 3

RESULTS AND DISCUSSION

3.1 CHARACTERIZATION

3.1.1 XRD Analysis

The PXRD results for Manganese oxide are displayed in Figure 3.1.1. The hexagonal $P6_3mc$ space group is represented by the peaks at 2θ angles of 36.6° and 42.5° . The hkl values of (111) and (200) can be applied to the reflection planes.

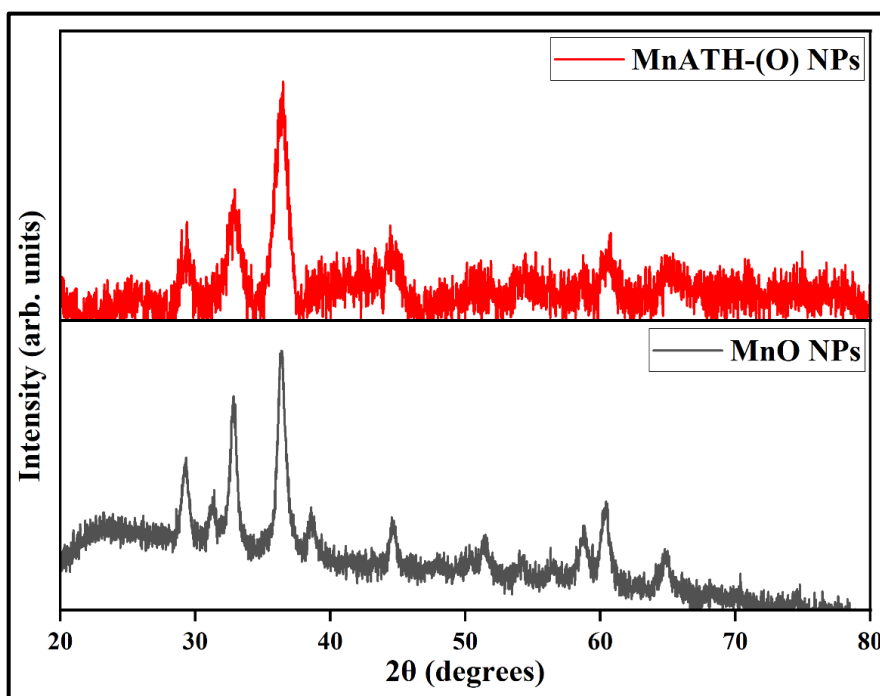


Figure 3.1.1. PXRD pattern of synthesized MnO NPs and MnATH-(O) NPs

The crystallite size of synthesized MnO NPs were calculated by Debye-Scherrer formula given below equation (2).

$$D = 0.94 \lambda / \beta \cos \theta \quad (2)$$

In this case, the wavelength is in Å, the FWHM is β (in radians), the average crystallinity is D , and the degree of diffraction is indicated by θ . The average crystallographic size (D) of the MnO NPs was determined to be 32.28 and 20.3 nm, respectively, using the Scherrer equation.

Phyto-fabricated metal oxide MnO NPs and MnATH-(O) NPs powder X-ray diffraction (PXRD) data are displayed in Figure 3.1.1.

3.1.2. FT-IR Analysis

The FTIR spectra of MnO NPs and MnATH-(O) NPs that were phyto-nanofabricated are shown in Figure 3.1.2 illustrates the stretching vibration of the O-H groups of water present as moisture, Hydroxyl Peaks 3400 cm^{-1} indicates the existence of OH groups that are surface-bound. Metal-oxygen (M-O) connections are confirmed to be present in the produced nanoparticles by the existence of bands in the $500\text{--}750\text{ cm}^{-1}$ provide strong indication of effective manganese oxide production. Hydroxyl Peaks 3400 cm^{-1} indicates the existence of OH groups that are surface-bound. Peaks of water 1630 cm^{-1} Frequently found in materials that are synthesized or kept in aqueous media.

Using a zeta potential analysis, the surface charge of the synthesized MnO NPs was also calculated and found to be -34.7 mV , indicating that MnATH-(O) NPs has a negative surface charge.

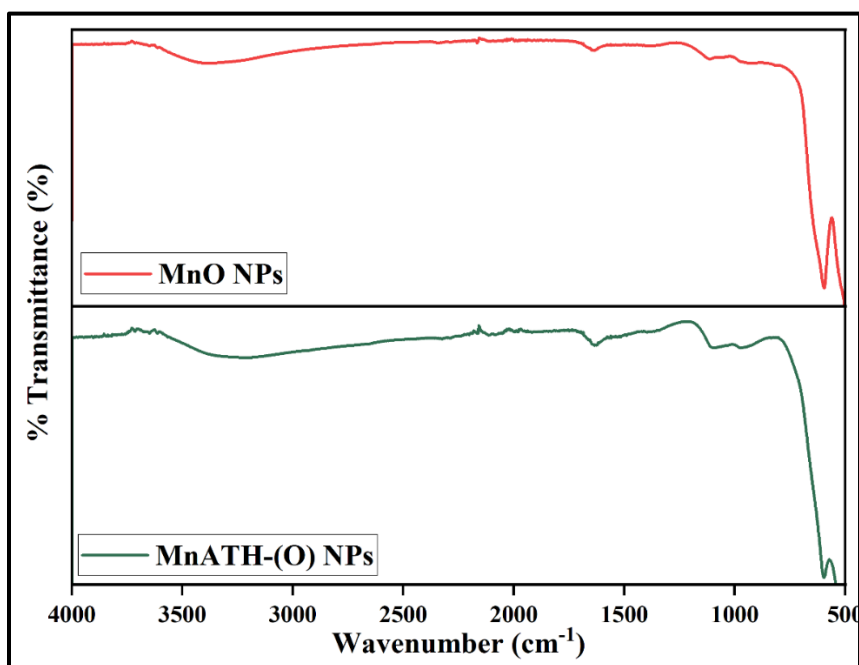
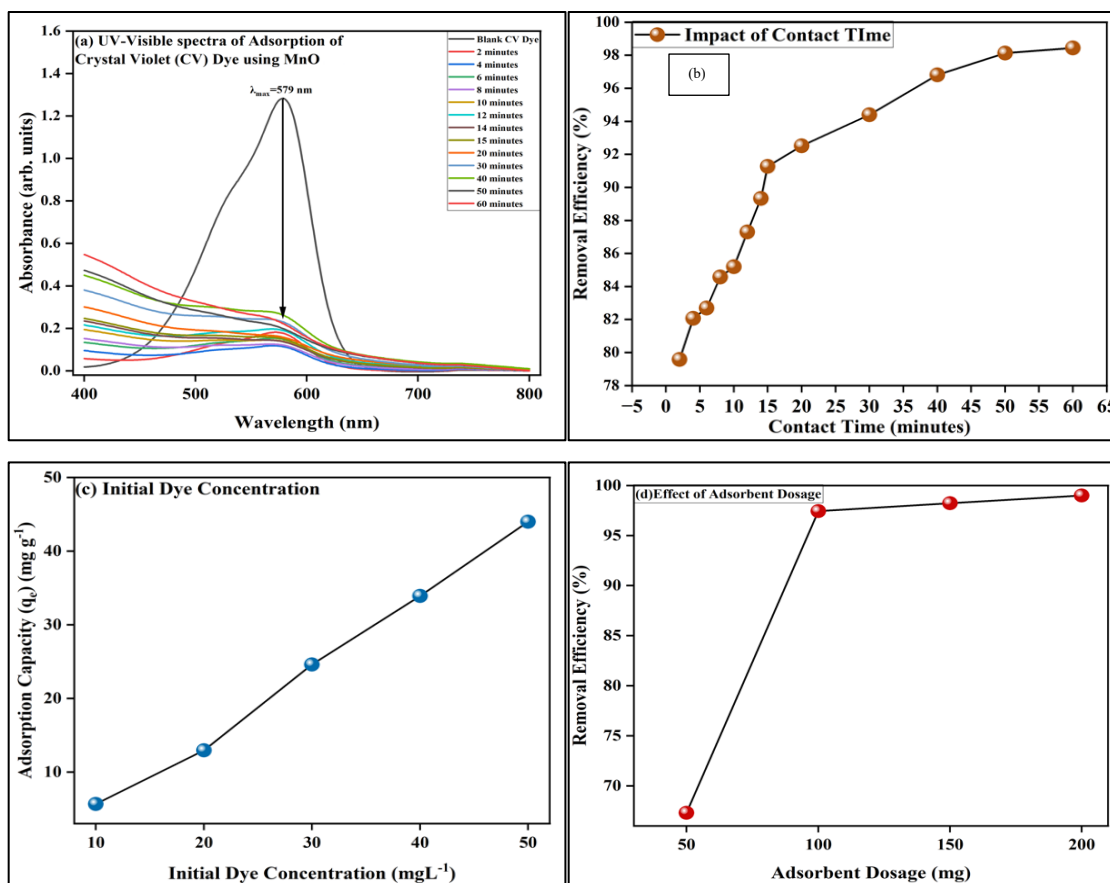


Figure 3.1.2. FTIR spectrum of synthesized MnO NPs and MnATH-(O) NPs

3.2.BATCH ADSORPTION EXPERIMENTS

It was investigated that how well synthesized MnATH-(O) NPs worked as adsorbent to remove cationic CV dye from aqueous solutions. MnATH-(O) NPs adsorptive efficacy for the uptake of Crystal violet (CV) dye was assessed in preliminary studies using 100 mg adsorbent (MnATH-(O) NPs) in 100 ml of dye solution containing 20 mg L^{-1} , Stirred under absence of light, a particular quantity of solution were taken out at regular intervals of 2 minutes. Then the solution were centrifuged at 4000 rpm for 10 minutes, at $\lambda_{\text{max}} = 579 \text{ nm}$ Using a UV visible spectrophotometer, the residual solution's concentration was determined. the results demonstrated an impressive removal efficiency in just 30 minutes. MnATH-(O) NPs were found to exhibit selective removal of cationic dyes.



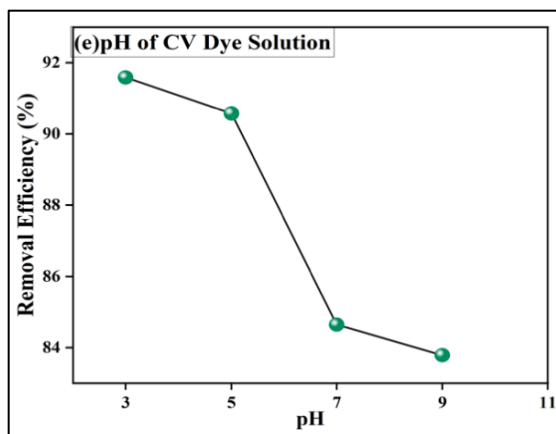


Figure 3.2.1 (a) UV Visible spectra of adsorption of CV dye using MnATH-(O) NPs, (b) influence of contact time on removal efficiency, (c) influence of initial dye concentration on adsorption capacity, (d) effect of adsorbent dosage on removal efficiency, (e) influence of pH on CV dye solution for removal efficiency

3.2.1.Impact of Contact time

In adsorption investigations involving the interaction of an adsorbent with a dye solution, experimental time is a crucial influencing aspect since it offers essential insights into the equilibrium state. The adsorption investigation examined the correlation between the percentage of CV sequestered over a 150-minute interval and the trial duration. For 60 minutes in the dark, 100 mg of adsorbent was agitated in 100 mL of A 20 mg L⁻¹ dose of CV dye solution with a pH of 3 in order to conduct the adsorption investigations. A Shimadzu1900i UV-vis spectrophotometer was used to record the absorbance spectra at $\lambda_{\text{max}} = 579$ nm after a set amount of solution was taken out at regular intervals of 15 minutes and centrifuged for 10 minutes at 4000 rpm. Using MnATH-(O) NPs as an adsorbent, Figure 3.2.1 shows the UV-visible spectra of CV dye over a wavelength range of 400–700 nm. The percentage elimination plotted against reaction time is shown in Figure 3.2.1. With 94.38% of the dye adsorbed in 30 minutes, the plot shows a sharp increase in the dye removal percentage was noted until 60 minutes, at which point the percentage removal efficiency peaked at 98.36%. The dye removal efficiency remained nearly constant after 60 minutes, showing that the saturation level had been reached, with no discernible rise. The presence of adsorption sites on the surface of NPs may help to explain these facts. First, there are a lot of open spots on the adsorbent surface where CV dye molecules can be adsorbed,

which leads to a high removal efficiency. Less adsorption sites are available on the adsorbent's surface as the experimental duration evolves, and as a result, the removal effectiveness decreases.

3.2.2 Impact of Initial CV concentration

By mixing 100 mg of adsorbent in 100 ml of aqueous solution of dye with different concentrations from 10 mg L⁻¹ to 50 mg L⁻¹ at pH 3 in the dark for 60 minutes. It was also possible to examine the impact of initial CV dye concentration on the adsorption capacity of MnATH-(O) NPs (Figure 3.2.1.c). It was shown that as the concentration of dye solution rose from 10 mg L⁻¹ to 50 mg L⁻¹, the adsorbent's adsorption capacity improved from 9.100 mg g⁻¹ to 49.039 mg g⁻¹. This occurs as a result of a larger mass transfer of CV dye molecules from the CV dye solution to the MnATH-(O) surface as a result of more frequent contacts between the molecules of the dye and the MnATH-(O) NPs surface at higher dye concentrations. CV dye molecules are more likely to separate from the solution phase and adsorb onto the surface of nanomaterials as a result of the rise in molecular collisions. Thus, it can be concluded that when the dye concentration rises from 10 mg L⁻¹ to 50 mg L⁻¹, MnATH-(O) NPs adsorption capability increases.

3.2.3. Impact of adsorbent dosage

To Study impact on adsorption using different doses of MnATH-(O) The influence of adsorbent amount on the effectiveness of CV dye removal was examined using NPs (50 mg, 100 mg, 150 mg, and 200 mg) in a 100 ml solution of CV dye.. The initial reaction duration (150 minutes) and CV dye concentration (20 mg L⁻¹) were all maintained at the same levels. In 150 minutes with 50 mg of adsorbent present, the removal effectiveness of MnATH-(O) NPs only reached 62.79%, as shown in Figure 3.2.1(d). It could be explained by the fact that there are less adsorption sites available for the uptake of CV dye from solution. Due to the abundance of active adsorption sites available for adsorption, a removal efficiency of over 98.90% was attained when the adsorbent dosage was increased to 100 mg, 150 mg, and 200 mg. Thus, it may be concluded that the ideal adsorbent dosage for CV dye uptake is 100 mg.

3.2.4 Impact of pH on CV dye solution

The adsorption mechanism of CV dye is significantly impacted by pH. 100 mL of a 20 mg L⁻¹ aqueous solution of CV dye with pH values ranging from 3 to 9 was used to investigate the effect

of pH on the adsorption of CV dye by 100 mg of MnATH-(O) NPs. The mixture was stirred for 60 minutes in the dark, the predetermined volume of solution was taken out every fixed interval of time 15 minutes. After that, the solutions were centrifuged for ten minutes at 4000 rpm. The absorbance was then estimated at $\lambda_{\max} = 579$ nm using a Shimadzu1900i UV-vis spectrophotometer. As the pH was raised from 3 to 9, the removal effectiveness of MnATH-(O) NPs rapidly decreased, going from 91.58% to 83.78% (Figure 3.2.1.e).

3.3. ADSORPTION KINETICS

The mechanics behind the adsorption process and the rate of adsorption are clearly understood thanks to adsorption kinetic studies. Adsorption tests utilizing 100 mg MnATH-(O) NPs in CV dye solution with a 20 mg L⁻¹ concentration were conducted in the dark for 150 minutes. By fitting experimental data to various kinetic models, such as the pseudo-first-order (PFO), pseudo-second-order (PSO), and Intraparticle Diffusion (IPD) models, the adsorption kinetics for CV adsorption on MnATH-(O) NPs were determined.

3.3.1. Lagergren pseudo-first-order (PFO) Adsorption Kinetics Model

This mechanism is commonly described by the Lagergren PFO model, Since the adsorption of solute from a liquid solution is a reversible interaction between the adsorbent and CV dye molecules. The variation in CV adsorption at time (t) directly affects the pace and concentration of CV dye elimination. The following represents the PFO model's linear regression:

$$\ln(q_e - q_t) = \ln q_e - k_1 t \quad (4)$$

Here, q_e and q_t (in mg g⁻¹), represent the adsorbent's dye absorption capacity at equilibrium and at a certain time t (in minutes), respectively. The symbol for the adsorption process's rate constant is k_1 (min⁻¹). k_1 and q_e can be found using the slope and intercept of the linear plot of $\ln q_e - q_t$ vs t .

3.3.2. Pseudo-second-order (PSO) Adsorption Kinetics Model

This model states that the quantity of active adsorption sites on the surface of MnATH-(O) NPs as well as the concentration of CV dye ions both affect the rate of adsorption. The surface adsorption process, which includes chemisorption and describes the extraction of the adsorbate

from a solution by physicochemical interactions between the two phases, is the step that determines the rate in this model. The following is a description of linear regression:

$$\frac{t}{q_t} = \frac{1}{k_2 q_e^2} + \frac{t}{q_e} \quad (5)$$

With,

$$h = k_2 q_e^2 \quad (6)$$

At time t , an adsorbent's capacity to absorb CV dye is shown by q_t (mg g^{-1}). cation's equilibrium rate constant is expressed as k_2 (min^{-1}). q_e represents the equilibrium dye adsorption capacity (mg g^{-1}). The initial adsorption rate ($\text{mg g}^{-1} \text{ min}^{-1}$) is denoted by h .

3.3.3 Intraparticle Diffusion (IPD) Adsorption Kinetics Model

The diffusion mechanism is clarified using the IPD model, which takes into account the creation of several layers according to Vanderwaal's forces, which is crucial for the growth of the physical adsorption process. The physical properties of the adsorbent, the dye solution's starting concentration, temperature, and rotation speed in batch mode are some of the factors that frequently affect the ID. The ID equation that Weber and Morris presented is as follows:

$$q_t = k_{id} t^{\frac{1}{2}} + C \quad (7)$$

Here, q_t (mg g^{-1}), indicates the adsorbent's ability to adsorb CV dye at time k_{id} ($\text{g mg}^{-1} \text{ min}^{-1/2}$), indicates the intraparticle diffusion rate coefficient, and C stands for the boundary layer's thickness. The slope of the q_t vs $t^{1/2}$ plot can be used to calculate the k_{id} values for each adsorbate (CV dye) concentration. As the adsorbate concentration rises, these values are seen to rise as well. Lower R^2 values of 0.94908 imply that IPD has no discernible effect on MnATH-(O) NPs ability to adsorb CV dye. However, the adsorption process might be controlled by a multi-step mechanism because there is not an intersection at the origin.

The adsorption kinetics plots are shown in Figure 3.3.1, and the estimated parameter values derived from the linear regressions of the previously described adsorption kinetic models are displayed in (Table 3.3.1.c) The experimental data was found to have a good correlation with the PSO model, having $R^2 = 0.9995$, indicating that the rate of CV adsorption by the MnATH-(O) NPs was mostly influenced by chemical adsorption. The parametric value of h was calculated using equation (6) and found to be $1.5675 \text{ mg g}^{-1} \text{ min}^{-1}$.

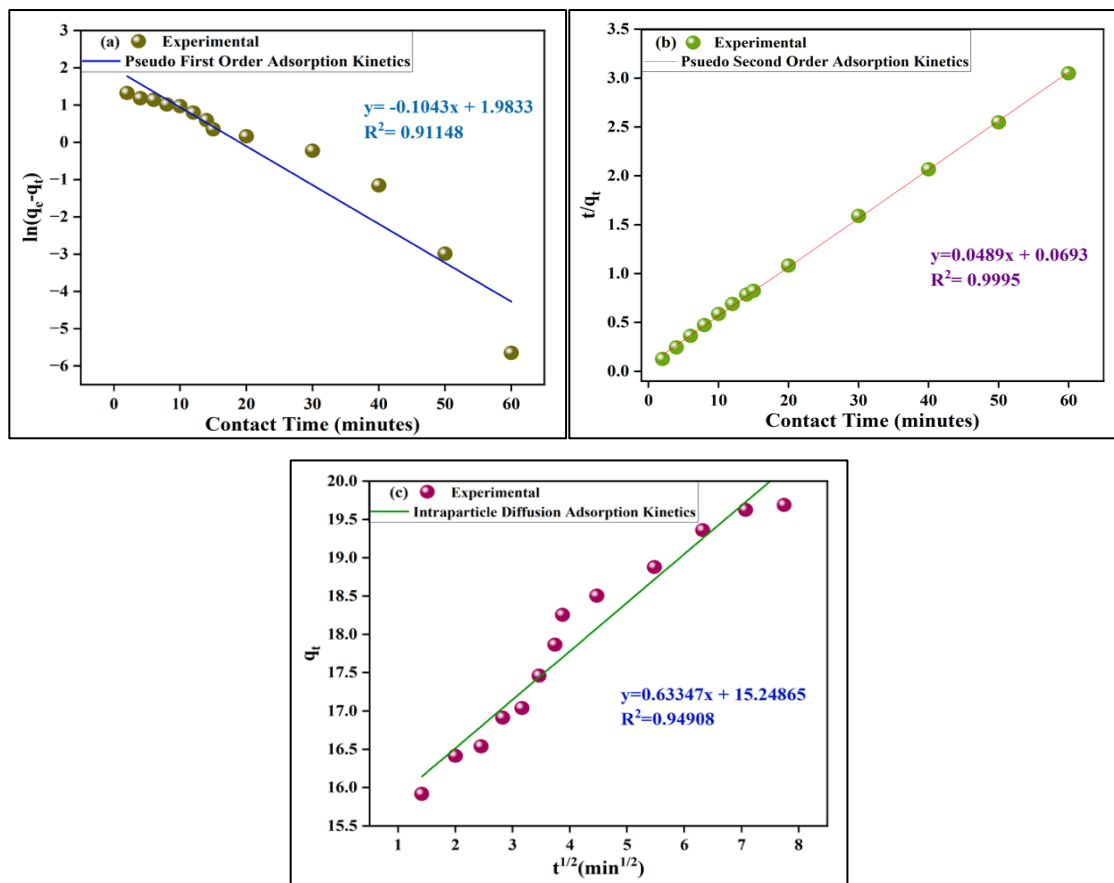


Figure 3.3.1 The linear adsorption kinetics curves that were fitted for CV dye adsorption by MnATH-(O) NPs using PFO, PSO AND IPD MODEL

Table 3.3.1. List of calculated parametric values for adsorption kinetics model for CV dye adsorption by MnATH-(O) NPs

Kinetic Models	Linear Plot	Parametric Values
Pseudo 1 st order $\ln(q_e - q_t) = \ln q_e - k_1 t$	$\ln(q_e - q_t) \text{ vs } t$	$R^2 = 0.91148$ $k_1 = 0.1043 \text{ min}^{-1}$ $q_e = 7.2667 \text{ mg g}^{-1}$
Pseudo 2 nd order $\frac{t}{q_t} = \frac{1}{k_2 q_e^2} + \frac{t}{q_e}$	$\frac{t}{q_t} \text{ vs } t$	$R^2 = 0.9995$ $k_2 = 0.00377 \text{ min}^{-1}$ $h = 1.5765 \text{ mg g}^{-1} \text{ min}^{-1}$ $q_e = 20.4498 \text{ mg g}^{-1}$
Intraparticle diffusion model $q_t = k_{id} t_{1/2} + C$	$q_t \text{ vs } t_{1/2}$	$R^2 = 0.94908$ $k_{id} = 0.63347 \text{ g mg}^{-1} \text{ min}^{-1/2}$ $C = 15.2486$

3.4 ADSORPTION ISOTHERM

Studies of Adsorption Isotherms In order to better understand the adsorption mechanism, provide specific information about the interactions between the adsorbent and adsorbate while evaluating the maximal dye adsorption capacity. The adsorption isotherms were examined using a CV dye solution containing concentrations between 10 and 50 mg L⁻¹ and 100 mg of adsorbent. The experimental results were analysed using three distinct isotherm models: the Langmuir, Freundlich, and Temkin models.

3.4.1. Langmuir Adsorption Isotherm Model

Langmuir's proposed model seeks to explain the saturated adsorption of adsorbate by the adsorbent in a monolayer manner on the homogenous surfaces of adsorbed materials. As a result, the molecules of the adsorbent don't interact with one another. The Langmuir model's linear regression is indicated by Equation (8):

$$\frac{C_e}{q_e} = \frac{1}{K_L q_{max}} + \frac{C_e}{q_{max}} \quad (8)$$

Where, the equilibrium CV concentration is denoted by C_e (mg L^{-1}) and the saturation adsorption capacity by q_e (mg g^{-1}), respectively. However, K_L (L mg^{-1}) and q_{max} (mg g^{-1}), stand for the Langmuir constant and maximal CV uptake capacity, respectively.

Another significant factor that shows the adsorption model's favorability and acceptability is the dimensionless separation factor (R_L). The adsorption process's validity is validated by the separation factor value. $R_L = 0$ indicates an irreversible reaction, $0 < R_L$ indicates a favourable reaction and $R_L = 1$ indicates a linear plot. These values have the following relationship:

$$R_L = \frac{1}{1 + K_L C_i} \quad (9)$$

The initial concentration of the CV solution is represented as mg L^{-1} by C_i , while the Langmuir constant is represented as K_L (L mg^{-1}).

3.4.2. Freundlich Adsorption Isotherm Model

According to the Freundlich adsorption isotherm model, adsorbate adsorption is non-ideal, occurs on a heterogeneous multilayer surface of the adsorbent (multilayer adsorption), and energies are distributed exponentially or non-uniformly to the active adsorption sites. The Freundlich isotherm model's linear regression is shown as

$$\ln q_e = \ln K_f + \frac{1}{n_f} \ln C_e \quad (10)$$

Here, q_e (mg g^{-1}), K_f [$(\text{mg g}^{-1}) (\text{L mg}^{-1})^{1/n_f}$], n_f , and C_e (mg L^{-1}), respectively, represent the adsorption capacity at equilibrium, Freundlich adsorption coefficient, adsorbate adsorption capability (heterogenic adsorption intensity), and CV concentration at equilibrium.

3.4.3. Temkin Adsorption Isotherm Model

The adsorption model that explains how the heat of adsorption affects the amount of surface covered is the Temkin isotherm. Because of the attractive or repulsive interactions between the adsorbed species, the heat of adsorption reduces as surface coverage rises. The Temkin adsorption isotherm model's linear regression is shown as

$$q_e = B \ln A_T + B \ln C_e \quad (11)$$

$$B = \frac{RT}{b} \quad (12)$$

The adsorption capacity at equilibrium, heat of adsorption constant, Temkin isotherm equilibrium constant, CV concentration at equilibrium, universal gas constant ($8.314 \text{ J K}^{-1}\text{mol}^{-1}$), absolute temperature, and the Temkin isotherm constant are represented by the following variables: , q_e (mg g^{-1}), B (J mol^{-1}), A_T , C_e (mg L^{-1}), R ($\text{J K}^{-1}\text{mol}^{-1}$), T (K), and b (mg L^{-1})

The slope and intercept of the plot of q_e against $\ln C_e$ are A_T and B , respectively.

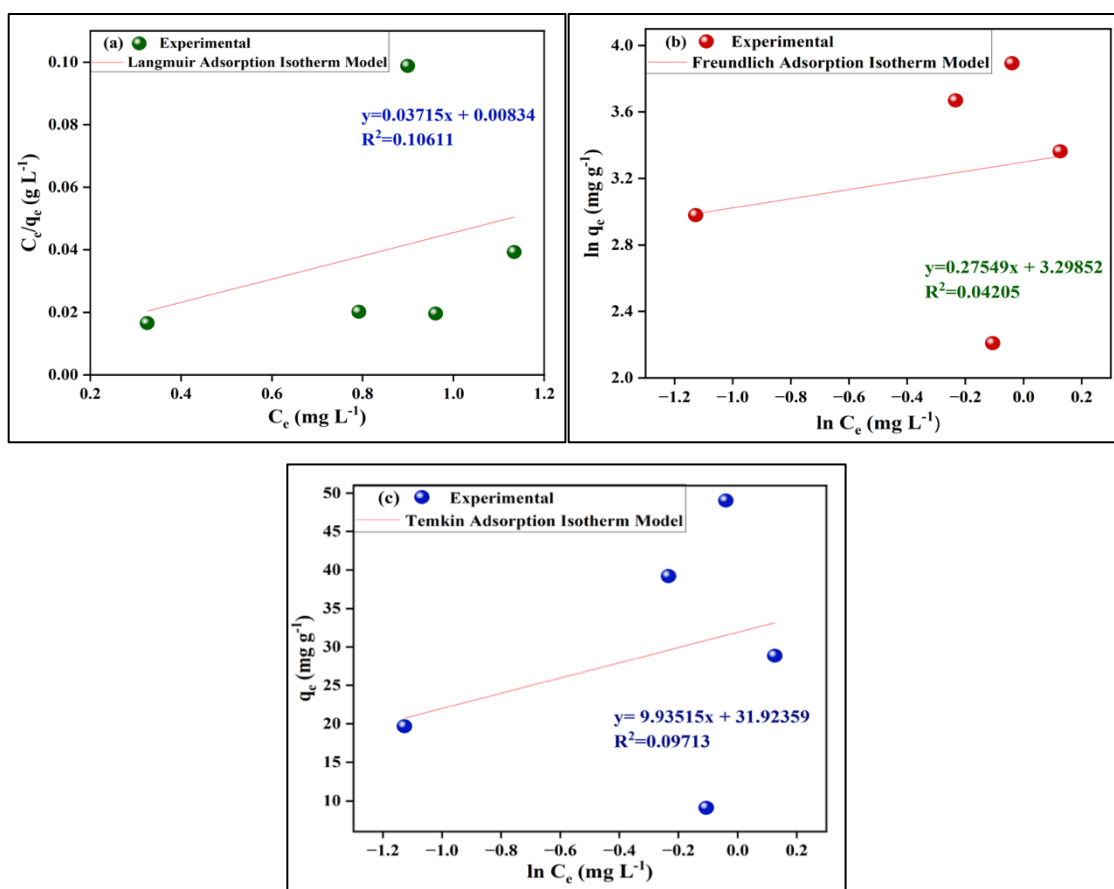


Figure 3.4.1 The graphs showing the linear connections between the Temkin, Freundlich, and Langmuir isotherm model

Table 3.4.1 Compilation of adsorption isotherm parametric values for several mathematical models

Isotherm Models	Linear Plot	Slope and intercept	Parametric Values
Langmuir Model $\frac{C_e}{q_e} = \frac{1}{k_L q_{max}} + \frac{C_e}{q_{max}}$	$\frac{C_e}{q_e} \text{ vs } C_e$	Slope = $\frac{1}{q_{max}} = 0.03715$ Intercept = $(\frac{1}{k_L q_{max}})$ = 0.00834	$R^2 = 0.10611$ $R_L = 0.01110$ $k_L = 4.4544 \text{ L mg}^{-1}$ $q_{max} = 26.9179 \text{ mg g}^{-1}$
Freundlich Model $\ln q_e = \ln K_f + \frac{1}{n_f} \ln C_e$	$\ln q_e \text{ vs } \ln C_e$	Slope = $\frac{1}{n_f} = 0.27549$ Intercept = $\ln K_f =$ 3.29852 mg g^{-1}	$R^2 = 0.04205$ $K_f = 27.0725 \text{ (mg g}^{-1}) \text{ (L mg}^{-1})^{1/n}$
Temkin Model $q_e = B \ln A_T + B \ln C_e$	$q_e \text{ vs } \ln C_e$	Slope = 9.93515 J/mol Intercept = $B \ln A_T$ = 31.92359 mg g^{-1}	$R^2 = 0.09713$ $A_T = 24.8584 \cdot 10^{-6}$ L g^{-1}

3.5.ADSORPTION THERMODYNAMICS

The thermodynamic factors explain the adsorption reaction's feasibility, spontaneity, and heat change, and they also evaluate the adsorption process spontaneity. To investigate the thermodynamics of the adsorption process, adsorption tests were conducted at four distinct temperatures: 313.15 K, 323.15 K, and 333.15 K. The entropy change (ΔS° , J mol⁻¹ K⁻¹) was computed by substituting the values of experimental adsorption data, the enthalpy change (ΔH° , kJ mol⁻¹), and the change in Gibbs free energy (ΔG° , kJ mol⁻¹). The slope and intercept of the linear plot of the enthalpy and entropy change yield the numerical values of $\ln\left(\frac{Q_e}{C_e}\right) \text{ vs } \frac{1}{T}$ or $\ln K_c \text{ vs } \frac{1}{T}$, respectively (Figure 3.6.1). Equations (13) and (14) explain how these values relate to one another.

$$\ln\left(\frac{Q_e}{C_e}\right) = -\left(\frac{\Delta H^\circ}{RT}\right) + \left(\frac{\Delta S^\circ}{R}\right) \quad (13)$$

$$\ln K_c = -\left(\frac{\Delta H^\circ}{RT}\right) + \left(\frac{\Delta S^\circ}{R}\right) \quad (14)$$

$$K_c = \frac{Q_e}{C_e} \quad (15)$$

Here, (ΔH , kJ mol⁻¹) and (ΔS° , J mol⁻¹ K⁻¹), respectively, stand for the enthalpy and entropy change, whereas K_c represents the thermodynamic equilibrium constant (L g⁻¹), which equivalent to $\frac{Q_e}{C_e}$,

The universal gas constant is represented by . R (8.314 × 10⁻³ kJ mol⁻¹ K⁻¹) and T(K) represents the temperature of the sorption system.

The following equation predicts the change in Gibbs free energy (ΔG° , kJ mol⁻¹) and the viability of the adsorption process:

$$\Delta G^\circ = -RT \ln K_c \quad (16)$$

Here, ΔG° , R, T, and $\ln K_c$ stand for the change in temperature (K), the universal gas constant (kJ mol⁻¹ K⁻¹), the thermodynamic equilibrium constant, and the Gibbs free energy (kJ mol⁻¹). The MnATH-(O) NPs surface CV adsorption was endothermic, as demonstrated by the ΔH° value (+ 39.0313 kJ mol⁻¹). Furthermore, as the reaction mixture's temperature rose, the negative values of ΔG° also rose (Table 3.5.1). This implies that the procedure is viable and thermodynamically stable, and that the rate of CV dye adsorption is high at higher temperatures. Nonetheless, the elevated spontaneity at the CV dye solution- interface was shown by the positive ΔS° value (+ 146.2133 J mol⁻¹ K⁻¹) Additionally, the spontaneity of the process is confirmed by the presence of a negative ΔG° value, whilst the positive connection between ΔG° and temperature suggests that the rate of adsorption rises as temperature rises.

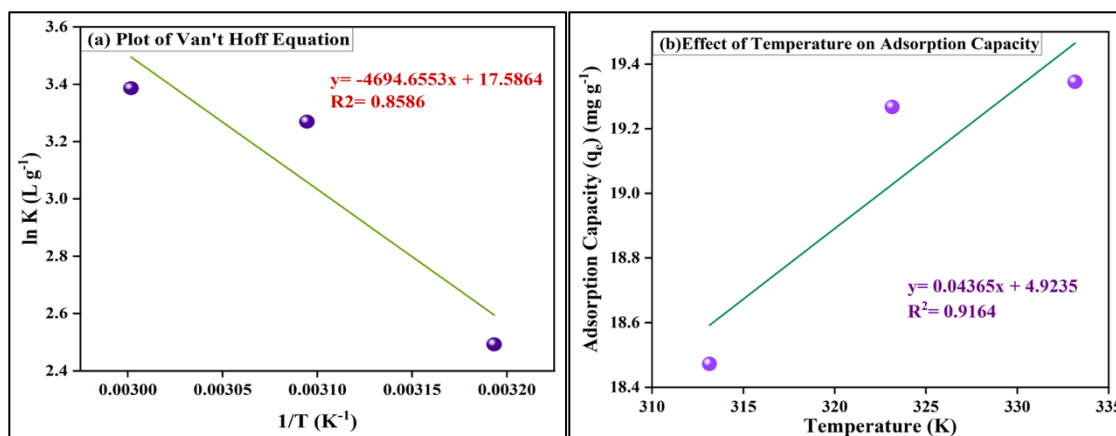


Figure 3.5.1 The Vant Hoff equation plot ($\ln K$ vs $1/T$) and the effect of temperature on adsorption capacity have been presented.

Table 3.5.1. Thermodynamic parametric values for CV dye adsorption by MnATH-(O) NPs

Temperature (K)	q_e (mg g ⁻¹)	ΔH° (kJ mol ⁻¹)	ΔS° (J mol ⁻¹ K ⁻¹)	ΔG° (kJ mol ⁻¹)
313.15	19.531	39.0313	146.2133	-9.302
323.15	19.577			-9.886
333.15	19.679			-10.951

CHAPTER 4

CONCLUSIONS AND FUTURE PROSPECTS

4.1 CONCLUSIONS

This study investigates the intriguing fabrication and application of MnATH-(O) NPs for the adsorption of crystal violet (CV) dye utilizing ATH extract. Significant properties of the MnATH-(O) NPs include their irregular shape, increased surface area, improved surface charge. These properties stood in sharp contrast to those of MnO NPs produced using the chemical co-precipitation technique.

This Anthocyanin mediated synthesis of manganese oxides (MnATH-(O) NPs) for applications in wastewater treatment. The physiochemical properties of the synthesized material were analysed using PXRD, FTIR, FESEM with EDX, The results indicate that the synthesized material has a crystallite size of 20.3 nm. It was investigated that how well synthesized MnATH-(O) NPs worked as adsorbent to remove cationic CV dye from aqueous solutions. Crystal violet (CV) dye was assessed in preliminary studies using 100 mg adsorbent (MnATH-(O) NPs) in 100 ml of dye solution containing 20 mg L⁻¹, under absence of light, at neutral pH, at $\lambda_{\text{max}} = 579$ nm, the results demonstrated an impressive removal efficiency with 94.38% of the dye adsorbed in just 30 minutes, the plot shows a sharp increase in the dye removal percentage was noted until 60 minutes, at which point the percentage removal efficiency peaked at 98.36%.

In conclusion, the Manganese oxide nanoparticles have been successfully synthesized by Green approach and used for the adsorption of CV dye. Since it leaves no hazardous traces and has several positive environmental impacts. This is a sustainable step towards the environment.

4.2 FUTURE PROSPECTS

The degradation of CV dye using green-synthesized MnO NPs has a bright future because it provides an environmentally responsible and sustainable way to address water contamination. MONPs can be produced in a green synthesis using algae, fungi, bacteria, and plant extracts. This technique minimizes the negative effects on the environment and cuts down on the use of dangerous chemicals. It has been shown that MONPs such as iron oxide, titanium dioxide, and zinc oxide significantly accelerate the degradation of CV dye. These nanoparticles high surface

area to volume ratio contributes to both their improved reactivity and photocatalytic activity. When dye molecules are exposed to light, nanoparticles catalyse the oxidation process, resulting in reactive oxygen species. Using green-synthesised metal oxide nanoparticles to decompose CV dye is an economical, highly effective, and low-toxicity method. This approach can potentially be scaled up for use in industrial settings. This method can be used to effectively purify water that has been contaminated with CV dye and other contaminants. It is also a sustainable and environmentally beneficial option that supports the objectives of circular economies and sustainable development. This brings us one step closer to a world free of pollution.

REFERENCES

- [1] R. Upadhyay, W. Przysaś, and B. Dave, “Myco-remediation of synthetic dyes: a comprehensive review on contaminant alleviation mechanism, kinetic study and toxicity analysis,” Jan. 01, 2024, *Springer Nature*. doi: 10.1007/s13762-024-05793-4.
- [2] S. Mani and R. N. Bharagava, “Exposure to crystal violet, its toxic, genotoxic and carcinogenic effects on environment and its degradation and detoxification for environmental safety,” in *Reviews of Environmental Contamination and Toxicology*, vol. 237, Springer New York LLC, 2016, pp. 71–104. doi: 10.1007/978-3-319-23573-8_4.
- [3] D. C. Roy *et al.*, “Biodegradation of Crystal Violet dye by bacteria isolated from textile industry effluents,” *PeerJ*, vol. 2018, no. 6, 2018, doi: 10.7717/peerj.5015.
- [4] R. Ahmad, “Studies on adsorption of crystal violet dye from aqueous solution onto coniferous pinus bark powder (CPBP),” *J Hazard Mater*, vol. 171, no. 1–3, pp. 767–773, Nov. 2009, doi: 10.1016/j.jhazmat.2009.06.060.
- [5] C. Puri and G. Sumana, “Highly effective adsorption of crystal violet dye from contaminated water using graphene oxide intercalated montmorillonite nanocomposite,” *Appl Clay Sci*, vol. 166, pp. 102–112, Dec. 2018, doi: 10.1016/j.clay.2018.09.012.
- [6] P. Karthik, S. Ravichandran, A. Mukkannan, and J. Rajesh, “Plant-mediated biosynthesis of zinc oxide nanoparticles from *Delonix Elata*: A promising photocatalyst for crystal violet degradation,” *Inorg Chem Commun*, vol. 146, p. 110122, Dec. 2022, doi: 10.1016/J.INOCHE.2022.110122.
- [7] S. Palamthodi, D. Kadam, and S. S. Lele, “Physicochemical and functional properties of ash gourd/bottle gourd beverages blended with jamun,” *J Food Sci Technol*, vol. 56, no. 1, pp. 473–482, Jan. 2019, doi: 10.1007/S13197-018-3509-Z/FIGURES/3.
- [8] “(PDF) Enhanced Extraction of Anthocyanins from Red Cabbage (*Brassica oleracea*) Using Microwave Assisted Extraction.” Accessed: Jun. 22, 2025. [Online]. Available: https://www.researchgate.net/publication/342242524_Enhanced_Extraction_of_Anthocyanins_from_Red_Cabbage_Brassica_oleracea_Using_Microwave_Assisted_Extraction
- [9] R. Mattioli, A. Francioso, L. Mosca, and P. Silva, “Anthocyanins: A Comprehensive Review of Their Chemical Properties and Health Effects on Cardiovascular and Neurodegenerative Diseases,” *Molecules* 2020, Vol. 25, Page 3809, vol. 25, no. 17, p. 3809, Aug. 2020, doi: 10.3390/MOLECULES25173809.
- [10] N. L. W. Septiani, B. Yuliarto, M. Iqbal, and Nugraha, “Synthesis of Zinc Oxide Nanoparticles using Anthocyanin as a Capping Agent,” *IOP Conf Ser Mater Sci Eng*, vol. 202, no. 1, p. 012070, May 2017, doi: 10.1088/1757-899X/202/1/012070.
- [11] H. K. Abdelhakim, E. R. El-Sayed, and F. B. Rashidi, “Biosynthesis of zinc oxide nanoparticles with antimicrobial, anticancer, antioxidant and photocatalytic activities by the endophytic *Alternaria tenuissima*,” *J Appl Microbiol*, vol. 128, no. 6, pp. 1634–1646, Jun. 2020, doi: 10.1111/jam.14581.
- [12] M. Batool, S. Khurshid, Z. Qureshi, and W. M. Daoush, “Adsorption, antimicrobial and wound healing activities of biosynthesised zinc oxide nanoparticles,” *Chemical Papers*, vol. 75, no. 3, pp. 893–907, Mar. 2021, doi: 10.1007/S11696-020-01343-7/FIGURES/11.
- [13] G. O. Akintayo *et al.*, “Synthesis, bioactivities and cytogenotoxicity of animal fur-mediated silver nanoparticles,” *IOP Conf Ser Mater Sci Eng*, vol. 805, no. 1, p. 012041, Mar. 2020, doi: 10.1088/1757-899X/805/1/012041.

- [14] S. Noreen *et al.*, “ZnO, CuO and Fe₂O₃ green synthesis for the adsorptive removal of direct golden yellow dye adsorption: Kinetics, equilibrium and thermodynamics studies,” *Zeitschrift für Physikalische Chemie*, vol. 235, no. 8, pp. 1055–1075, Aug. 2021, doi: 10.1515/ZPCH-2019-1599/ASSET/GRAPHIC/J_ZPCH-2019-1599_FIG_007.JPG.
- [15] J. O. Adeyemi, D. C. Onwudiwe, and A. O. Oyediji, “Biogenic Synthesis of CuO, ZnO, and CuO–ZnO Nanoparticles Using Leaf Extracts of *Dovyalis caffra* and Their Biological Properties,” *Molecules* 2022, *Vol. 27, Page 3206*, vol. 27, no. 10, p. 3206, May 2022, doi: 10.3390/MOLECULES27103206.
- [16] S. G. Firisa, G. G. Muleta, and A. A. Yimer, “Synthesis of Nickel Oxide Nanoparticles and Copper-Doped Nickel Oxide Nanocomposites Using *Phytolacca dodecandra* L’Herit Leaf Extract and Evaluation of Its Antioxidant and Photocatalytic Activities,” *ACS Omega*, vol. 7, no. 49, pp. 44720–44732, Dec. 2022, doi: 10.1021/ACSOMEGA.2C04042.
- [17] S. M. Abdelbasir, D. A. Rayan, and M. M. Ismail, “Synthesis of Cu and CuO nanoparticles from e-waste and evaluation of their antibacterial and photocatalytic properties,” *Environmental Science and Pollution Research* 2023 30:38, vol. 30, no. 38, pp. 89690–89704, Jul. 2023, doi: 10.1007/S11356-023-28437-5.
- [18] S. Yadav, P. Singh, G. Varshney, Saurabh, P. Singh, and R. Kaur, “Photocatalytic degradation of crystal violet dye using phytofabricated zinc oxide nanoparticles from anthocyanin extract,” *Microchemical Journal*, vol. 213, p. 113681, Jun. 2025, doi: 10.1016/J.MICROC.2025.113681.



AAKASH

thesis PLAGUE CHECK.docx



Delhi Technological University

Document Details

Submission ID

trn:oid::27535:101769521

Submission Date

Jun 20, 2025, 9:52 AM GMT+5:30

Download Date

Jun 20, 2025, 9:53 AM GMT+5:30

File Name

thesis PLAGUE CHECK.docx

File Size

19.5 MB

31 Pages

5,912 Words

32,920 Characters







10% Overall Similarity

The combined total of all matches, including overlapping sources, for each database.




Filtered from the Report

- Bibliography
- Quoted Text
- Cited Text
- Small Matches (less than 10 words)

Match Groups

-  **47 Not Cited or Quoted 10%**
Matches with neither in-text citation nor quotation marks
-  **0 Missing Quotations 0%**
Matches that are still very similar to source material
-  **0 Missing Citation 0%**
Matches that have quotation marks, but no in-text citation
-  **0 Cited and Quoted 0%**
Matches with in-text citation present, but no quotation marks

Top Sources

- 7%  Internet sources
- 6%  Publications
- 5%  Submitted works (Student Papers)

Integrity Flags





0 Integrity Flags for Review

No suspicious text manipulations found.




Our system's algorithms look deeply at a document for any inconsistencies that would set it apart from a normal submission. If we notice something strange, we flag it for you to review.

A Flag is not necessarily an indicator of a problem. However, we'd recommend you focus your attention there for further review.

Match Groups

-  **47 Not Cited or Quoted 10%**
Matches with neither in-text citation nor quotation marks
-  **0 Missing Quotations 0%**
Matches that are still very similar to source material
-  **0 Missing Citation 0%**
Matches that have quotation marks, but no in-text citation
-  **0 Cited and Quoted 0%**
Matches with in-text citation present, but no quotation marks

Top Sources

- 7%  Internet sources
- 6%  Publications
- 5%  Submitted works (Student Papers)

Top Sources

The sources with the highest number of matches within the submission. Overlapping sources will not be displayed.

1	Publication	Sarla Yadav, Pooja Singh, Gunjan Varshney, Saurabh, Poonam Singh, Raminder K...	2%
2	Internet	www.deswater.com	<1%
3	Internet	www.researchgate.net	<1%
4	Internet	www.mdpi.com	<1%
5	Internet	baadalsg.inflibnet.ac.in	<1%
6	Internet	kijoms.uokerbala.edu.iq	<1%
7	Internet	www.jkcs.or.kr	<1%
8	Internet	assets.researchsquare.com	<1%
9	Internet	datapdf.com	<1%
10	Internet	www.coursehero.com	<1%

11	Internet	core.ac.uk	<1%
12	Internet	www.shd.org.rs	<1%
13	Internet	d.docecity.com	<1%
14	Internet	worldwidescience.org	<1%
15	Publication	Ngoc Chung Le, Dinh Van Phuc. " Sorption of lead (II), cobalt (II) and copper (II) io...	<1%
16	Internet	coek.info	<1%
17	Submitted works	National Tsing Hua University on 2025-06-19	<1%
18	Submitted works	University of Malaya on 2011-01-23	<1%
19	Submitted works	University of St Andrews on 2024-10-18	<1%
20	Internet	pubs.rsc.org	<1%
21	Internet	systems.enpress-publisher.com	<1%
22	Publication	Mohammednur Abdu, Saeideh Babae, Abebe Worku, Palesa Diale, Titus A.M. Ms...	<1%
23	Internet	alumni-portal.sasin.edu	<1%
24	Internet	eprints.uniska-bjm.ac.id	<1%



25	Internet	espace.curtin.edu.au	<1%
26	Submitted works	Anna University on 2025-03-06	<1%
27	Submitted works	National Institute of Technology, Rourkela on 2014-11-17	<1%
28	Submitted works	Universiti Teknologi Malaysia on 2012-02-08	<1%
29	Internet	bbrc.in	<1%
30	Internet	es.scribd.com	<1%
31	Internet	etheses.whiterose.ac.uk	<1%
32	Internet	locus.ufv.br	<1%
33	Internet	mjs.uomustansiriyah.edu.iq	<1%

